A Study of the Radio Channel for Low Earth Orbit Telecommunication Satellites

Cláudio G. Batista, Ana C. S. Souza and Gustavo F. Rodrigues

***Abstract*— This study conducts a first-order statistical analysis of the radio channel between a Low Earth Orbit (LEO) satellite and a ground station. We used measurements from the TinyGS project's open-access database, which included data from four satellites. The classical Loo and Lutz models were applied to generate Cumulative Distribution Function (CDF) curves. The simulations and experimental data were statistically compared using the Kolmogorov-Smirnov (KS) test and Wasserstein distance metrics. Additionally, the K-Nearest Neighbors (KNN) algorithm was employed to estimate new input parameters for the Loo model, improving the accuracy of the results for the scenarios under investigation.**

***Keywords*— LEO (Low Earth Orbit) satellite, statistical modeling of the radio channel, KNN method parameter estimation.**

I. Introduction

In recent decades, investments in the space industry have grown exponentially, with modern satellites delivering increasingly sophisticated services [1]. A significant shift has been observed from using geostationary satellites (GEO - Geostationary Earth Orbit, altitude: 35,786 km) to non-geostationary – particularly Medium Earth Orbit (MEO, altitude: 7,000-25,000 km) and LEO (Low Earth Orbit, altitude: 500-2,000 km) [2]. The demand for high-throughput and low-latency applications has driven growing interest in LEO satellites [3]. Current LEO constellations provide broadband services (e.g., Starlink, Iridium, OneWeb), Internet of Things (IoT) applications (e.g., Hiber, Mytriota) and PNT (Position, Navigation and Timing) systems [1]. Among LEO platforms, CubeSats have emerged as a particularly notable standard [4].

The manufacturing and orbital deployment of LEO satellites are simpler and more cost-effective compared to traditional satellites. These systems also offer greater flexibility in constellation configuration. However, their size and weight limitations restrict onboard equipment and power capacity [5]. Another challenge is the relative motion between the satellite and ground station, which induces Doppler effects and time-varying signal fading, particularly for stations surrounded by obstacles (buildings, trees, topography, etc) [5],[6]. Consequently, characterizing the radio channel between ground stations and satellites is critical for system design and optimization. This analysis can leverage models commonly used in mobile satellite communication systems, known as Land Mobile Satellite (LMS) channels. Traditional LMS models assume a mobile ground station and a geostationary (GEO) satellite, with temporal signal variations modeled through statistical probability distributions [2], [7]-[11]. These account for both shadowing (slow/large-scale fading) and multipath effects (fast/small-scale fading). For LEO satellite systems, where the ground station is fixed and the satellite is in motion, prior studies have adapted LMS models [4]-[7] and results indicate that fading effects remain prevalent [4], [9].

This work presents a first-order statistical modeling of the LEO satellite radio channel. We used measurements from the TinyGS project, a collaborative open-access database [12], which aggregates data from globally distributed ground stations operating under standardized hardware and software configurations [13]. The received signal was analyzed using Loo [10], [14] and Lutz model [11], [15] which are established techniques in LMS systems. The resulting Cumulative Distribution Functions (CDFs) were compared with empirical data through Kolmogorov-Smirnov (KS test) [16] and Wasserstein distance (WS distance) [17]. Furthermore, we employed the K-Nearest Neighbors (KNN) algorithm [18] to estimate optimized parameters for the Loo model. This approach yielded improved modeling accuracy and identified novel input parameters.

II. Low Earth Orbit Satellites (LEO satellites)

A. Overview

LEO satellites typically operate at altitudes h between 500 and 2,000 km, exhibiting continuous motion relative to points fixed on Earth. Their orbits are generally elliptical with very low eccentricity, approximating circular trajectories. Unlike geostationary (GEO) satellites, LEO orbital planes not necessarily coincide with the equatorial plane. The relative angle between these planes is termed the inclination angle i. LEO satellites complete one Earth revolution in approximately tens of minutes, with ground station visibility windows lasting just a few minutes. The elevation angle θ – defined between the local ground station plane and the satellite – determines this visibility period, where the range (θ_{min} to θ_{max}) specifies the observable duration for a given satellite. Figure 1 illustrates this geometry, with the station-satellite distance d referred to as the $slant\ range$.

As an illustrative example, a satellite at 900 km altitude with 45^o inclination orbits at a relative velocity of 7.402 km/s (26,647 km/h), completing one revolution in 102 minutes. For a ground station with elevation angles between 10^o and 50^o, the satellite remains visible for 11.8 minutes. To maintain uninterrupted signal coverage, LEO systems employ satellite

Cláudio G. Batista, Ana C. S. Souza and Gustavo F. Rodrigues, Laboratório Integrado de Sistemas Espaciais (LISE), Universidade Federal de São João del-Rei (UFSJ), Ouro Branco-MG, e-mail:claudiog@ufsj.edu.br, aclaudia@ufsj.edu.br and gfernandes@ufsj.edu.br.

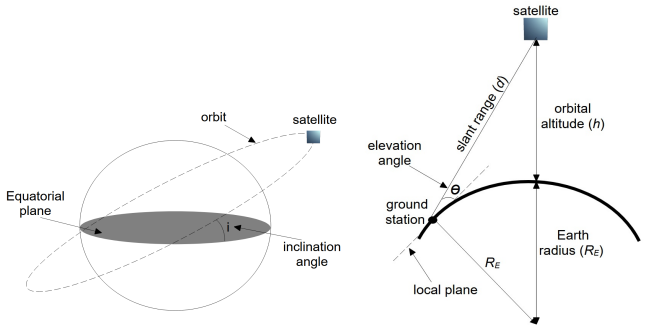

(a) (b)

Fig. 1. (a) LEO orbital characteristics. (b) Satellite-ground station geometry.

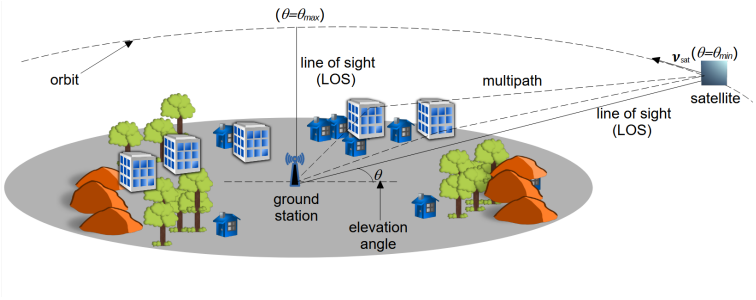

Fig. 2. Ground station surrounded by obstacles illustrating the received signal fading effects.

networks called constellations, which additionally provide global coverage. Readers are referred to [3] and [4] for further details on LEO and CubeSat systems.

B. Radio Communication Channel

LEO satellite systems operate across multiple frequency bands including VHF (30-300 MHz), UHF (300 MHz-3 GHz), L-band (1-2 GHz), S-band (2.2-3.4 GHz) among others [1]. Due to size and weight constraints, satellite transmission power typically ranges between 0 to 40 dBm, with antenna gains generally near 0 dBi. This study focuses specifically on UHF signals from CubeSat satellites. In future works, the authors plan to also investigate signals at higher frequencies.

Consequently, radio channel analysis must account for: (a) carrier frequency shifts due to satellite relative motion (Doppler effect), and (b) temporal amplitude fluctuations of the received signal. These amplitude variations result from dynamic slant range variations (d) and combined shadowing (slow fading) and multipath effects (fast fading) [7]. Both fading phenomena occur when ground stations operate in obstructed environments (urban structures, vegetation, terrain topography, etc.). Slow fading arises from alternating Line-Of-Sight (LOS) and Non-Line-Of-Sight (NLOS) conditions, while fast fading stems from constructive/destructive interference of multipath components [19] (see Figure 2). These effects are intensified at small elevation angles ($\theta < 25^o$) [5].

Various techniques for Doppler shift estimation and compensation are well-documented in the literature [1],[4]. The analysis of signal fading effects employs statistical characterization through Probability Density Functions (PDFs) and Cumulative Distribution Functions (CDFs) [2], [7]-[11],[19].

III. Statistical Models for the Radio Channel

A. Loo's Model

The model proposed by Chun Loo [10],[14] is one of the most widely used in LMS communication systems due to its flexibility and ability to incorporate diverse signal propagation conditions [9]. It assumes that the total received signal is a combination of slow fading (modeled by a Log-normal distribution [19]) and fast fading (estimated by a Rice distribution [19]). The probability density function (PDF) of the total received signal r is the joint PDF of these two effects and is given by:

$$PDF_{Loo}(r) = \frac{r}{b_0\sqrt{2\pi d_0}} \int_0^\infty \frac{1}{z} \exp\left[-\frac{(\ln(z)-\mu)^2}{2d_0}\right] \cdot \exp\left[-\frac{(r^2+z^2)}{2b_0}\right] I_0\left(\frac{rz}{b_0}\right) dz \quad (1)$$

where r represents the linear voltage amplitude of the received signal, μ is the mean and $\sqrt{d_0}$ the standard deviation of the Log-normal shadowing. The parameter b_0 denotes the average power of the scattered signal component due to multipath effects, and $I_0(...)$ is the zeroth-order modified Bessel function of the first kind.

To obtain the CDF, equation (1) must be integrated over the interval from the required signal level R to infinity (probability that $r > R$):

$$CDF_{Loo}(R) = \int_R^\infty PDF_{Loo}(r)dr = 1 - \int_0^R PDF_{Loo}(r)dr \quad (2)$$

and equation 2 leads to a complicated double integral that requires numerical evaluation.

Loo's model is classified as a single-state model. The literature has proposed multi-state models [9], where different scenarios are defined according to the behavior of the received signal. The strategy involves using distinct PDFs for each state and combining them according to specific criteria [2]. In a two-state model, it is common to associate a GOOD state (for line-of-sight conditions with minimal shadowing) and a BAD state (for non-line-of-sight conditions with dominant multipath effects) [5]. Models with three or more states have also been developed [2], [6].

B. Lutz Model

The framework proposed by E. Lutz *et. al* [11],[15] is a two-state model, defining a *GOOD* state for high-power received signals (LOS with minimal shadowing) and a *BAD* state for low-power signals (NLOS with significant shadowing). Multipath effects are considered in both states. The states are linearly combined through a parameter A representing the percentage of time in the *BAD* state.

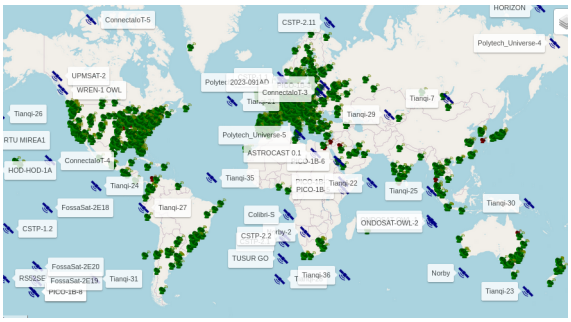

Fig. 3. Interface display of the TinyGS platform showing ground station locations and the observed LEO satellites.

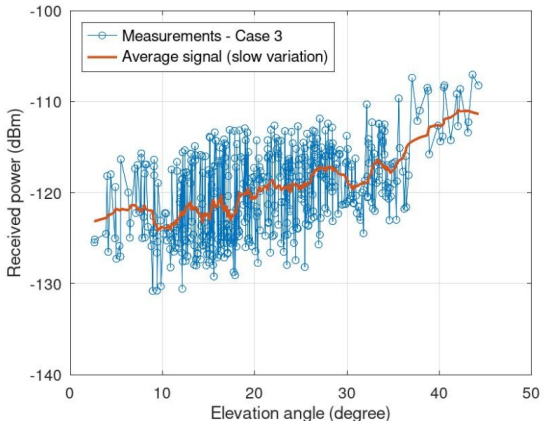

Fig. 4. Received power measurements from multiple ground stations for Case 3, corresponding to satellite TIANQI-07.

Following the authors' original notation in [11] and [15], the signal s represents the received power, and the *PDF* for the *GOOD* state follows a Rice distribution:

$$PDF_G(s) = c\exp\left[-c(s+1)\right] I_0\left(2c\sqrt{s}\right) \tag{3}$$

where c (linear) represents the ratio of the line-of-sight power to the multipath-received power (Rice factor). For the *BAD* state, a combined Rayleigh distribution [19] and Log-normal distribution is adopted, expressed as:

$$PDF_B(s) = \frac{10}{\sqrt{2\pi}\sigma_L \ln(10)} \int_0^\infty \frac{1}{s_0^2} \exp\left(-\frac{s}{s_0}\right) \cdot \exp\left[-\frac{(10\log(s_0) - \mu_L)^2}{2\sigma_L^2}\right] ds_0 \tag{4}$$

where μ_L is the mean and σ_L the standard deviation (both in dB) due to Log-normal shadowing. The final *PDF* of the Lutz model is given by:

$$PDF_{Lutz}(s) = (1-A)\cdot PDF_G(s) + A \cdot PDF_B(s) \tag{5}$$

The cumulative probability distribution is calculated as:

$$CDF_{Lutz}(S) = 1 - \int_0^S PDF_{Lutz}(s)ds \tag{6}$$

which must also be evaluated numerically.

IV. Measurements and Results

A. Measurements and TinyGS Project

The authors used data from LEO satellites through the open-access TinyGS project [12], [13]. TinyGS establishes a standard for relatively low-cost ground station hardware and software, thereby forming a network of ground stations. Then, the measurement data is concentrated on a single platform. Figure 3 shows a global distribution map of the project's ground stations. The system comprehensively provides observational data pertaining to low-Earth orbit satellites, including but not limited to orbital altitude, elevation angle relative to the receiving station, and the satellite-to-ground station distance. Furthermore, it delivers signal characterization metrics encompassing received power levels, Signal-to-Noise Ratio (SNR) measurements, and Doppler shift phenomena.

In this scenario, data were collected through an API (Application Programming Interface) between October and December 2024. For the current study, measurements in the 400 MHz band were selected, corresponding to 4 LEO satellites identified in Table I. For each satellite, a set of ground stations with similar characteristics (antenna height and type, radio receiver, etc.) were chosen, all located in medium urban environments, resulting in 4 distinct cases for analysis.

TABLE I
CHARACTERISTICS OF THE OBSERVED LEO SATELLITES.

Satellite/ NORAD	Frequency (MHz)	Mean altitude(km)	Inclination (degree)
NORBI/46494	436.70	492.25	97.8
NORBY-02/57179	435.60	540.45	97.6
TIANQI-07/54687	400.45	467.25	97.6
TIANQI-28/59912	400.45	904.75	45.0

Statistical characterization of the received signal power was performed as a function of the elevation angle θ, observing each ground station's antenna radiation pattern. Since fading effects are most pronounced at low elevation angles, only data points with $\theta < 45^o$ were considered. As an illustrative example, Figure 4 shows the received signal for Case 3, corresponding to satellite TIANQI-07.

B. Results

The analysis involved estimating the CDF of the measured data and comparing it with both Loo and Lutz models. Additionally, the Rice distribution [19] is included as it represents the characteristic signal behavior under line-of-sight conditions with multipath effects. Table II presents the input parameters for each model, maintaining the original notation from [14] and [15]. Each parameter set was obtained from the literature [9], [10], corresponding to scenarios closely matching the measurement conditions described in Section IV-A. Specifically, parameters were selected based on the closest operating

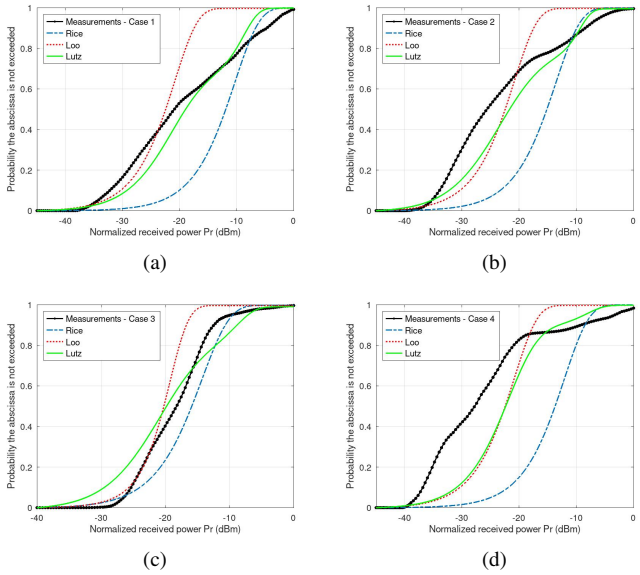

Fig. 5. Cumulative distribution functions (CDFs) comparing measured data with theoretical models: (a) Case 1, (b) Case 2, (c) Case 3 and (d) Case 4

frequency, the most similar ground station environment and comparable propagation conditions.

TABLE II
INPUT PARAMETERS FOR EACH MODEL AND STATISTICAL TESTS.

Case/Model	Parameters	KS	WS
Case 1			
Loo	μ=-0.69 $\sqrt{d_0}$=0.23 b_0=0.251	0.392	0.128
Lutz	A=0.66 c=6.0 dB μ_L=-11.0 dB σ_L=2.8 dB	0.144	0.058
Case 2			
Loo	μ=-0.69 $\sqrt{d_0}$=0.23 b_0=0.251	0.340	0.109
Lutz	A=0.78 c=9.3 dB μ_L=-12.0 dB σ_L=4.4 dB	0.124	0.074
Case 3			
Loo	μ=-0.115 $\sqrt{d_0}$=0.161 b_0=0.126	0.433	0.075
Lutz	A=0.8 c=5.5 dB μ_L=-10.0 dB σ_L=3.7 dB	0.155	0.066
Case 4			
Loo	μ=-0.74 $\sqrt{d_0}$=0.19 b_0=0.299	0.381	0.151
Lutz	A=0.89 c=3.9 dB μ_L=-12.0 dB σ_L=2.0 dB	0.206	0.13

Figure 5 presents the comparative analysis results between empirical measurements and theoretical models. The Lutz model demonstrates superior agreement with experimental data for Cases 1 and 2, consistently outperforming alternative approaches. Case 3 reveals more complex behavior, with neither model maintaining clear dominance as both periodically approximate the measured values at different elevation ranges. For Case 4, the Loo and Lutz models generate nearly indistinguishable CDF curves, suggesting comparable performance under these specific propagation conditions. To quantitatively assess these observations, statistical validation was performed using the Kolmogorov-Smirnov test (KS) [16] for distributional similarity and the Wasserstein (WS) distance metric [17] for evaluating probabilistic divergences, providing robust numerical confirmation of the visual findings.

The non parametric KS test determines the maximum vertical distance between two cumulative distribution functions $F(x)$ and $G(x)$ serving as a sensitive indicator of local distributional differences. The test is computed as follows [16]:

$$KS = \max_x \left(|F(x) - G(x)|\right) \tag{7}$$

The WS distance represents a fundamental metric for comparing CDFs, particularly valuable for capturing nuanced differences in distributional shape, location, and dispersion. The first-order metric is formally defined as [17]:

$$WS = \int_{-\infty}^{\infty} |F(x) - G(x)| dx \tag{8}$$

The output range for both tests spans from 0 (indicating identical distributions) to 1 (representing completely dissimilar distributions). Table II presents the obtained values for all analyzed cases. Overall, the Lutz model demonstrated superior performance across most scenarios. This outcome can be attributed to the model's more sophisticated formulation and additional input parameters, which provide greater flexibility.

C. Parameter Estimation

To enhance the statistical channel modeling accuracy, we focused on optimizing the input parameters for the Loo model. The simultaneous estimation of the three parameters μ, $\sqrt{d_0}$ and b_0 proves to be computationally challenging given the inherent nonlinearity of equation (1). This motivated the adoption of the K-Nearest Neighbors (KNN) machine learning algorithm, a versatile method applicable to both classification and regression problems. The KNN approach operates by analyzing the spatial proximity of data points, where predictions for new observations are derived from the weighted characteristics of their K closest neighbors. In classification contexts, the algorithm deterministically assigns each point to the predominant class among its nearest neighbors.

This study generated 10,000 synthetic CDF samples using the Loo model, with training parameters randomly sampled from the following ranges: $-5 < \mu < 7$, $0 < \sqrt{d_0} < 3$ and $0 < b_0 < 3$, as illustrated in Figure 6. The data set was partitioned into training (80%) and testing (20%) subsets, with the KNN regression configured to consider $k = 10$ nearest neighbors. For each new CDF input, the algorithm identified the 10 most similar training curves using the Wasserstein distance metric, then computed the weighted average of their parameters for prediction.

The optimized parameters derived through the KNN algorithm are presented in Table III, while Figure 7 demonstrates the improved CDFs achieved. Quantitative validation using both the KS test and WS distance metrics (Table III) revealed statistically significant improvements over baseline parameters. A significant improvement is observed with the new parameters, suggesting they are more suitable for the analyzed LEO satellite scenarios.

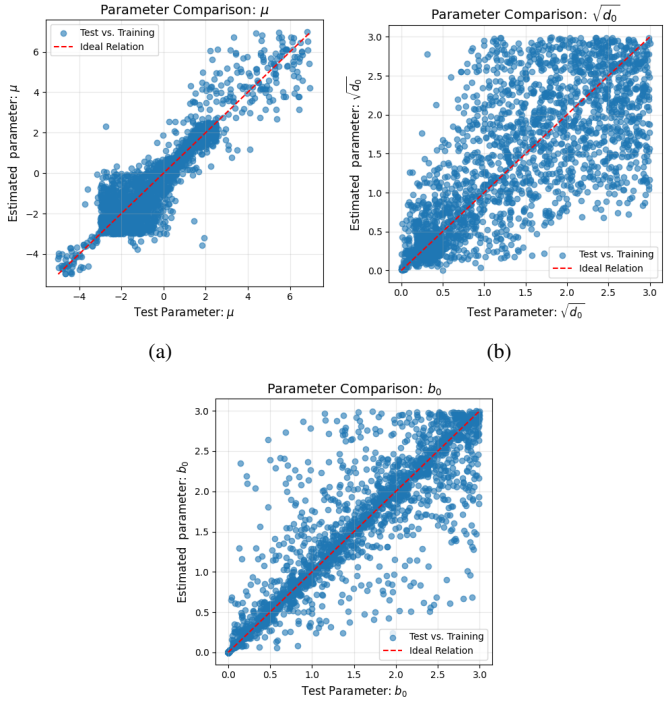

Fig. 6. Parameter Estimation Training phase using KNN Algorithm (a) μ, (b) $\sqrt{d_0}$ and (c) b_0.

TABLE III

ESTIMATED INPUT PARAMETERS AND TESTS FOR THE LOO MODEL.

Case	Estimated parameters	KS	WS
1	μ=−0.441 $\sqrt{d_0}$=2.120 b_0=0.158	0.130	0.360
2	μ=−0.848 $\sqrt{d_0}$=1.360 b_0=0.124	0.093	0.056
3	μ=−0.115 $\sqrt{d_0}$=0.761 b_0=0.351	0.110	0.019
4	μ=−1.060 $\sqrt{d_0}$=0.732 b_0=0.015	0.361	0.065

V. CONCLUSIONS

This work analyzed LEO satellite-ground station radio channels using statistical methods. We adopted the Loo and Lutz models - originally developed for traditional LMS systems - to measurements in UHF band, validating their effectiveness for LEO scenarios through Kolmogorov-Smirnov and Wasserstein distance metrics. A KNN-optimized version of the Loo model showed improved accuracy, better matching experimental data. These results confirm these models' utility for LEO systems when properly parameterized. The approach provides a basis for developing adaptive models for next-generation satellite networks. In future works, the authors plan to also investigate signals at higher frequencies (L and S bands).

REFERENCES

[1] F. S Prol, R. M. Ferre *et. al* "Position, Navigation, and Timing (PNT) Through Low Earth Orbit (LEO) Satellites: A Survey on Current Status, Challenges, and Opportunities," *IEEE Communications Surveys and Tutorials*, v. 10, pp. 83971-84002, 2022.

[2] M. Tropea and F. De Rango "A Comprehensive Review of Channel Modeling for Land Mobile Satellite Communications," *MDPI Electronics*, v. 11, no.5,2022.

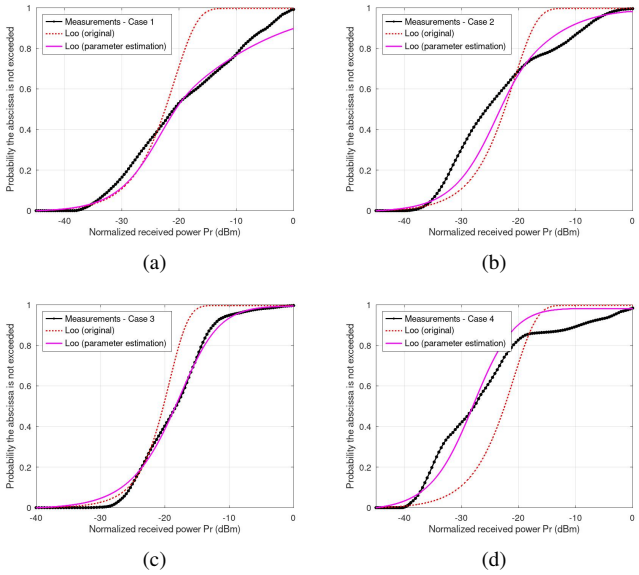

Fig. 7. New CDFs derived from the estimated parameters for (a) Case 1, (b) Case 2, (b) Case 3 and (b) Case 4.

[3] O. Kodheli, E. Lagunas *et. al* "Satellite Communications in the New Space Era: A Survey and Future Challenges," *IEEE Communications Surveys and Tutorials*, v. 23, no.1, pp. 70-109, 2021.

[4] N. Saeed, A. Elzanaty *et. al* "CubeSat Communications: Recent Advances and Future Challenges," *IEEE Communications Surveys and Tutorials*, v. 22, no.3, pp. 1839-1862, 2020.

[5] J. J. L. Salamanca, L. O. Seman *et. al* "Finite-State Markov Chains Channel Model for CubeSats Communication Uplink," *IEEE Trans. on Aerospace and Electronic Systems*, v. 56, no.1, pp. 142-154, 2020.

[6] M. Aslnia, M. Soleimani *et. al* "Statistical channel modeling for low-elevation in LEO satellite communication," *Elsevier Results in Engineering*, v. 23, pp. 102494, 2024.

[7] Victor M. Baeza, Eva Lagunas *et. al* "An Overview of Channel Models for NGSO Satellites ," *2022 IEEE 96th Vehicular Technology Conference (VTC2022)*, pp. 1-6, 2022.

[8] Y. Lee and J. P. Choi "Performance Evaluation of High-Frequency Mobile Satellite Communications," *IEEE Access*, pp. 49077-49087, 2019.

[9] F. P. Fontan, A. Mayo *et. al* , "Review of generative models for the narrowband land mobile satellite propagation channel," *Int. Journal of Satellite Communications and Net.*, v. 26, no.4, pp. 291-316 , 2008.

[10] C. Loo and J. S. Butterworth, "Land mobile satellite channel measurements and modeling," *Proceedings of the IEEE*, v. 86, no.7 , pp. 1442-1463, 1998.

[11] E. Lutz , "Modelling of the land mobile satellite communications channel," *2013 IEEE-APS Topical Conference on Antennas and Propagation in Wireless Communications (APWC)*,, pp. 199-202, 2013.

[12] TinyGS WEB Appication. Available online: https://tinygs.com (accessed on october-december 2024).

[13] J. S. Gomes and A. F. da Silva "TinyGS vs. SatNOGS: A Comparative Analysis of Open-Source Satellite Ground Station Networks," *MDPI Telecom*, v. 5, no.1 , pp. 228-254, 2024.

[14] C. Loo, "A statistical model for a land mobile satellite link," *IEEE Transactions on Vehicular Technology*, v. 34, no.3, pp. 122–127, 1985.

[15] E. Lutz, *et. al*, "Land mobile satellite channel measurements and modeling," *IEEE Trans. on Vehicular Technology*, v.40, no.2, 1991.

[16] F. J. Massey , "The Kolmogorov-Smirnov Test for Goodness of Fit," *Journal of the American Stat. Association*, v.46, no.253, pp.68-78, 1951.

[17] S. S. Vallender , "Calculation of the Wasserstein Distance Between Probability Distributions on the Line," *Theory of Probability & Its Applications*, v. 18, no.4, pp. 784-786 , 1974.

[18] T. M. Grile *et. al* "Improved Methods for Distribution Identification and Regression Parameter Estimation in a Satellite Reliability Application," *IEEE Transactions on Reliability*, pp. 1-13, 2024.

[19] F. P. Fontan and P. Mariño Espiñeira, *Modeling the Wireless Propagation Channel*. John Wiley and Sons, 2008.